The Nitrosyl Azide Potential Energy Hypersurface: A High-Energy-Density Boom or Bust?

John Morrison Galbraith* and Henry F. Schaefer III

Contribution from the Center for Computational Quantum Chemistry, The University of Georgia, Athens, Georgia 30602

Received October 10, 1995. Revised Manuscript Received March 20, 1996[⊗]

Abstract: Motivated by the recent isolation and spectroscopic characterization of nitrosyl azide (N_4O), we have undertaken an *ab initio* investigation of the originally reported structure as well as various structural isomers on the potential energy hypersurface. Geometries and harmonic vibrational frequencies have been predicted for the *trans*-chain isomer along with the 6 π electron potentially aromatic ring structure with various levels of theory up through the triple-ζ plus double polarization single and double excitation coupled cluster (TZ2P CCSD) method and the multireference configuration interaction method (MRCISD). In addition, estimates are made for extension to higher levels of theory, arriving at final predictions of $r_e(ON_1) = 1.176$ Å, $r_e(N_1N_2) = 1.472$ Å, $r_e(N_2N_3) = 1.272$ Å, $r_e(N_3N_4) < 1.130$ Å, $\Theta_e(ON_1N_2) = 110.5°$, $\Theta_e(N_1N_2N_3) = 105.4°$, $\Theta_e(N_2N_3N_4) = 174.5°$, and $r_e(ON_1) < 1.389$, $r_e(N_1N_2) < 1.250$, $r_e(N_3N_4) > 1.423$, $\Theta_e(N_1ON_4) = 106.3°$ for the *trans*-chain and ring isomers, respectively. Energy relationships, bond lengths, vibrational frequencies, Mulliken bond indices, and molecular orbital arguments are used to elucidate nitrogen oxide bonding. While the ring isomer is predicted to be the most stable structure on the hypersurface, the barrier to dissociation is most likely between 1 and 2 kcal mol^{-1} (including zero-point vibrational energy [ZPVE], the existence of any barrier becomes questionable) making isolation theoretically possible but experimentally difficult. This small barrier also detracts from the attractiveness of the N_4O ring structure as a high-energy-density material. The *trans*-chain isomer, however, lies in an energy valley with higher sides, consistent with its previous experimental observation.

I. Introduction

Many nitrogen-containing compounds decompose to yield chemically inert N_2 with large releases of energy. For purposes of energy storage, such compounds are sought which are substantially higher in energy than their decomposition products but with activation barriers sufficient for safe handling. A possible candidate is nitrosyl azide (N_4O), an unstable oxide of nitrogen whose decomposition products would be "virtually pure hot air"[1] thus making it an ideal, environmentally friendly high-energy propellant.

Attempts to produce nitrosyl azide date back to the beginning of this century.[2] While the isotopic labeling experiments of Clusis and Effenberger[3] apparently showed N_4O to exist as a reaction intermediate (eq 1), isolation remained elusive. In their

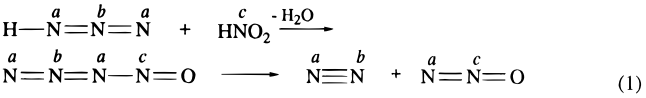

(1)

four-part study on the mechanism of the azide nitrite reaction, Stedman and co-workers[4] concluded that while nitrosyl azide plays a key role in many reactions, it always immediately breaks down into N_2O and N_2.

In view of the instability of N_4O, Lucien[5] approached the problem via low-temperature techniques. In spite of numerous explosions, low yields, and other experimental difficulties, a yellowish substance was produced at temperatures below −30 °C. This substance was identified as nitrosyl azide based on decomposition studies and "inferences" from infrared (IR) absorption spectra. This assignment remained unconfirmed until recently when Schultz, Tornieporth-Oetting, and Klapötke[6] combined theory with experiment in a study that drew the attention of a semipopular review.[1,7] Following a procedure similar to that of Lucien, Schultz *et al*. also produced a pale yellow solid. The Raman spectrum of this solid was then taken and compared to theoretical harmonic vibrational frequencies derived from second-order Møller−Plesset perturbation theory (MP2) with a 6-31+G* Gaussian basis set. The outstanding agreement of the scaled MP2/6-31G* frequencies with experiment led to the unequivocal assignment of this substance as an open *trans*-chain N_4O species with four nitrogens and a terminal oxygen.

With 6 π electrons, the N_4O ring system is a candidate for aromatic stabilization. There have been numerous discussions of the aromaticity of analogous systems in the literature,[8] most dealing with all-carbon systems and slight variations thereof, but no studies concerning the N_4O five-membered ring have appeared to date. While Schultz *et al*. predicted the ring isomer to be 13.7 kcal mol^{-1} more stable than the *trans*-chain isomer,[9] the ring isomer was determined to be a short-lived intermediate in the decomposition of the *trans*-chain isomer into N_2 and N_2O.[10]

* E-mail address: johnnyg@tabalos.ccqc.uga.edu.

[⊗] Abstract published in *Advance ACS Abstracts,* May 1, 1996.

(1) Fletcher, E. A. *Chem. Eng. News* **1993**, *71* (51), 2.
(2) Werner, T. *Proc. R. Soc. London* **1991**, *28*, 257.
(3) Clusis, K.; Effenberger, E. *Helv. Chim. Acta* **1955**, *38*, 1843.
(4) Stedman, G. *J. Chem. Soc.* **1959**, 1702, 2943, 2949. Bunton, C. A.; Stedman, G. *J. Chem. Soc.* **1959**, 3466.
(5) Lucien, H. W. *J. Am. Chem. Soc.* **1958**, *80*, 4458.
(6) Schultz, A.; Tornieporth-Oetting, I. C.; Klapötke, T. M. *Angew. Chem., Int. Ed. Engl.* **1993**, 32, 1610.
(7) Stinson, S. *Chem. Eng. News* **1993**, *71* (48), 51.
(8) Badgor, G. M. *Aromatic Character and Aromaticity*; Cambridge University Press: London, 1969. Streitwieser, A., Jr. *Molecular Orbital Theory for Organic Chemists*; Wiley: New York, 1961 and references therein.
(9) Klapötke, T. M.; Schultz, A. *Chem. Ber.* **1995**, *128*, 201.
(10) Tornieporth-Oetting, I. C.; Klapötke, T. M. *Angew. Chem., Int. Ed. Engl.* **1995**, *34*, 511.

S0002-7863(95)03415-9 CCC: $12.00

The related hexazene (N_6) system would seem a reasonable target for investigation, because it is isoelectronic with the ubiquitous, extensively characterized benzene ring. Despite much experimental[11] and theoretical[12] work, the existence of the N_6 system remains in doubt. Moving from the more localized C−H σ bond electrons in benzene to the diffuse nitrogen lone pairs in N_6 introduces a destabilizing effect which counters any benefit from the delocalized π electrons of the ring. This finding is in accord with the works of Shaik, Hiberty, Lefour, Ohanessian[13] and Jug and Köster,[14] which attribute the stability of "aromatic" systems to σ effects rather than π delocalization. Either way, the N_6 potential energy hypersurface (PES) is extremely flat.

One step closer to the N_4O system is the pentazole anion (N_5^-). Although the all-carbon analog, cyclopentadienyl anion ($C_5H_5^-$), is known to be important in transition metal chemistry, forming metal sandwich compounds such as ferrocene [$(C_5H_5)_2$-Fe],[15] the pentazole anion has never been isolated. Nguyen, Elguéro, and co-workers[16] studied this molecule and the $N_2 + N_3^- \rightarrow N_5^-$ PES using *ab initio* techniques. In addition to predicting harmonic vibrational frequencies, they concluded that N_5^- should be isolable in an inert matrix at low temperatures. They also concluded, on the basis of extended Hückel calculations, that N_5^- metal sandwich complexes should exist.

Some other systems of interest for their similarity to the ring structure of N_4O are furan (C_4H_4O) and the pentazoles (N_4R). Furan is a well-known organic compound, and as a result, it has been studied extensively both theoretically[17] and experimentally.[18] As pointed out above for the C_6H_6/N_6 comparison, moving from C_4H_4O to N_4O is expected to be accompanied by a loss in stabilization. A few pentazoles have been isolated,[19] representing the only all-nitrogen "aromatic" rings in existence. However, the parent pentazole, (N_5H), which is isoelectronic with N_4O, has not been isolated[20] despite *ab initio* predictions that it represents a minimum on the PES.[21] It is hoped that concepts developed concerning the bonding in these and other five-membered heterocycles[17] will be applicable to the N_4O system as well.

II. Methods

The smallest basis set used in this study consists of the standard Huzinaga−Dunning−Hay[22] double-ζ set of contracted Gaussian functions with the addition of a set of d-type polarization functions to each atom.[23] This (9s5p1d/4s2p1d) basis is designated as DZP. Diffuse s- and p-type functions were added to the DZP basis (DZP^{++}) in order to more accurately describe the dissociation PES.[24] A larger, more flexible basis was constructed from the Huzinaga−Dunning[25] triple-ζ basis set with the addition of two d-type polarization functions to each atom.[26] This (10s6p2d/5s3p2d) basis is designated TZ2P.

Because electron correlation has been shown to be essential for the description of nitrogen rings,[12] self-consistent-field (SCF) optimizations[27] were performed only to locate starting structures for correlated levels on the N_4O PES and are not reported herein. In addition, the two-configuration SCF[28] (TCSCF) method was needed to treat the linear $^1\Delta$ state (see below). Initially correlation effects were included via the configuration interaction including the single and double excitation (CISD)[29] method. In order to account for the lack of size consistency in CI procedures, N_2 plus N_2O was considered as a supermolecule. In addition, the single and double excitation coupled cluster (CCSD)[30] and CCSD with perturbative inclusion of triple excitation [CCSD(T)][31] methods were used. For all correlated procedures, the five lowest lying molecular orbitals corresponding to the 1s-type orbitals on each atom were held doubly occupied (five frozen core), and the five highest virtual orbitals were kept unoccupied (five deleted virtuals).

Multireference CISD (MRCISD) energy points at the DZP CISD optimized geometries were also found and compared to CCSD and CCSD(T) energy points at the same geometries. One difficulty of MRCISD procedures is choosing an appropriate reference space. This is particularly a problem in the present situation where the structures in question have vastly differing geometries and therefore no clear correspondence between respective excitations. Following the procedure of Grev and Schaefer[32] modified by Fermann, Sherill, Crawford, and Schaefer,[33] CI natural orbitals (CINOs) were generated and all reference configurations with coefficients above a certain threshold level were included in the MRCISD. Thresholds were chosen at 0.040 (MRCISD-A) and 0.030 (MRCISD-B). MRCISD-B required 11, 12, 11, 12, and 15 references and 3 660 251, 8 215 932 , 3 471 158, 2 151 978, and 5 789 832 configurations for the N_4O structures shown in Figures 1, 2, 3, 4 and 5, respectively.

All structures were completely optimized within the given symmetry constraints to 10^{-6} au in Cartesian coordinates using analytic gradient techniques. The SCF force constants and normal vibrations were determined by analytic second-derivative procedures,[34] while all correlated force constants and molecular vibrational frequencies were determined by the method of finite differences of analytic gradients.

(11) Vogler, A.; Wright, R. E.; Kunkely, H. *Angew. Chem., Int. Ed. Engl.* **1980**, *19*, 717.

(12) Lauderdale, W. J.; Stanton, J. F.; Bartlett, R. J. *J. Phys. Chem.* **1992**, *96*, 173. Engelke, R. *J. Phys. Chem.* **1992**, *96*, 10789. Saxe, P.; Schaefer, H. F. *J. Am. Chem. Soc.* **1983**, *105*, 1760. Huber, H.; Ha, T.-K.; Nguyen, M. T. *J. Mol. Struct. (THEOCHEM)* **1983**, *105*, 351. Ha, T.-K.; Cimiragilia, R.; Nguyen, M. T. *Chem. Phys. Lett.* **1981**, *83*, 317.

(13) Shaik, S. S.; Hiberty, P. C.; Lefour, J.-M.; Ohanessian, G. *J. Am. Chem. Soc.* **1987**, *109*, 363.

(14) Jug, K.; Köster, A. M. *J. Am. Chem. Soc.* **1990**, *112*, 6772.

(15) Lauher, J. W.; Hoffmann, R. *J. Am. Chem. Soc.* **1976**, *98*, 1729. Holloway, J. D. L.; Geiger, W. E., Jr. *J. Am. Chem. Soc.* **1979**, *101*, 2038.

(16) Nguyen, M. T.; McGinn, M. A.; Hegarty, A. F.; Elguéro, J. *Polyhedron* **1985**, *4*, 1721. Nguyen, M. T.; Sana, M.; Leroy, G.; Elguéro, J. *Can. J. Chem.* **1982**, *61*, 1435.

(17) Cordell, F. R.; Boggs, J. E. *J. Mol. Struct. (THEOCHEM)* **1981**, *48*, 329. Cordell, F. R.; Boggs, J. E. *J. Mol. Struct. (THEOCHEM)* **1988**, *164*, 175. Hilal. R. *J. Comput. Chem.* **1980**, *1*, 348. Hilal, R. *J. Comput. Chem.* **1980**, *1*, 358. Bernardi, F.; Bottoni, A.; Venturini, A. *J. Mol. Struct. (THEOCHEM)* **1988**, *163*, 173.

(18) Fourme, R. *Acta Crystallogr., Sect. B* **1972**, *28*, 2984. Mata, F.; Martin, M. C.; Sorensen, G. O. *J. Mol. Struct. (THEOCHEM)* **1978**, *48*, 157. Barge, B.; Christensen, D.; Hansen-Nyguard, L.; Rastrup-Andersen, J.; Dixon, W.; Schottlander, M. *J. Mol. Spectrosc.* **1956**, *9*, 124.

(19) Huisgen, R.; Ugi, I. *Angew. Chem.* **1956**, *68*, 705. Wallis, J. D.; Dunitz, J. D. *J. Chem. Soc., Chem. Commun.* **1983**, *16*, 910.

(20) Janoschek, R. *Angew. Chem., Int. Ed. Engl.* **1993**, *32*, 230.

(21) Ferris, K. F.; Bartlett, R. J. *J. Am. Chem. Soc.* **1992**, *114*, 8304.

(22) Huzinaga, S. *J. Chem. Phys.* **1965**, *42*, 1923. Dunning, T. H.; Hay, P. J. In *Modern Theoretical Chemistry*; Schaefer, H. F., Ed.; Plenum: New York, 1977; Vol. 3, p 1 ff.

(23) $\alpha_d(O) = 0.85$, $\alpha_d(N) = 0.80$.

(24) $\alpha_s(O) = 0.082\,270$, $\alpha_p(O) = 0.065\,080$, $\alpha_s(N) = 0.060\,290$, $\alpha_p(N) = 0.051\,480$: Lee, T. J.; Schaefer, H. F. *J. Chem. Phys.* **1985**, *83*, 1784.

(25) Dunning, T. H. *J. Chem. Phys.* **1970**, *53*, 2823. Dunning, T. H. *J. Chem. Phys.* **1971**, *55*, 716.

(26) $\alpha_d(O) = 1.70$, $\alpha_d(O) = 0.425$, $\alpha_d(N) = 0.40$ $\alpha_d(N) = 0.40$.

(27) Pulay, P. *Adv. Chem. Phys.* **1987**, *69*, 241. Pulay, P. In *Modern Theoretical Chemistry*; Schaefer, H. F., Ed.; Plenum: New York, 1977; Vol. 4, pp 153−185. Yamaguchi, Y.; Osamura, Y.; Goddard, J. D.; Schaefer, H. F. *A New Dimension to Quantum Chemistry*; Oxford University Press: New York, 1994.

(28) Osamura, Y.; Yamaguchi, Y.; Schaefer, H. F. *J. Chem. Phys.* **1982**, *77*, 383. Yamaguchi, Y.; Osamura, Y.; Schaefer, H. F. *J. Am. Chem. Soc.* **1983**, *105*, 7506.

(29) Brooks, B. R.; Laidig, W. D.; Saxe, P.; Goddard, J. D.; Yamaguchi, Y.; Schaefer, H. F. *J. Chem. Phys.* **1980**, *72*, 4652. Osamura, Y.; Yamaguchi, Y.; Schaefer, H. F. *J. Chem. Phys.* **1981**, *75*, 2919. Osamura, Y.; Yamaguchi, Y.; Schaefer, H. F. *J. Chem. Phys.* **1982**, *77*, 383. Rice, J. E.; Amos, R. D.; Handy, N. C.; Lee, T. J.; Schaefer, H. F. *J. Chem. Phys.* **1986**, *85*, 963.

(30) Purvis, G. D.; Bartlett, R. J. *J. Chem. Phys.* **1982**, *76*, 1910. Scuseria G. E.; Scheiner, A. C.; Lee, T. J.; Rice, J. E.; Schaefer, H. F. *J. Chem. Phys.* **1987**, *86*, 2881. Scuseria, G. E.; Janssen, C. L.; Schaefer, H. F. *J. Chem. Phys.* **1988**, *89*, 7382. Scheiner, A. C.; Scuseria, G. E.; Rice, J. E.; Schaefer, H. F. *J. Chem. Phys.* **1987**, *87*, 5361.

(31) Raghavachari, K.; Trucks, G. W.; Pople, J. A.; Head-Gordon, M. *Chem. Phys. Lett.* **1989**, *157*, 479. Sucseria, G. E.; Lee, T. J. *J. Chem. Phys.* **1991**, *94*, 442.

(32) Grev, R. S.; Schaefer, H. F. *J. Chem. Phys.* **1992**, *96*, 6850.

(33) Fermann, J. T.; Sherill, C. D.; Crawford, T. D.; Schaefer, H. F. *J. Chem. Phys.* **1994**, *100*, 8132.

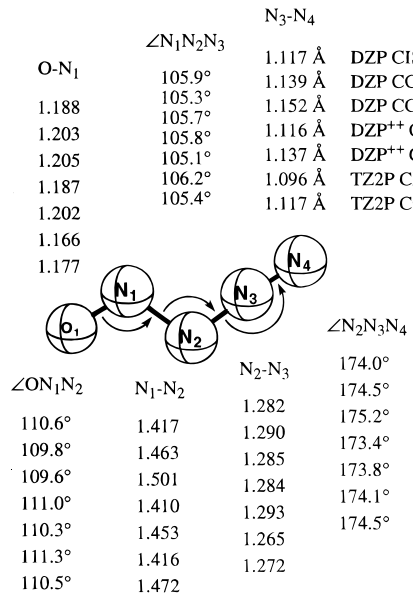

Figure 1. Predicted geometrical parameters for the C_s-symmetry $\tilde{X}\ ^1A'$ *trans*-chain isomer.

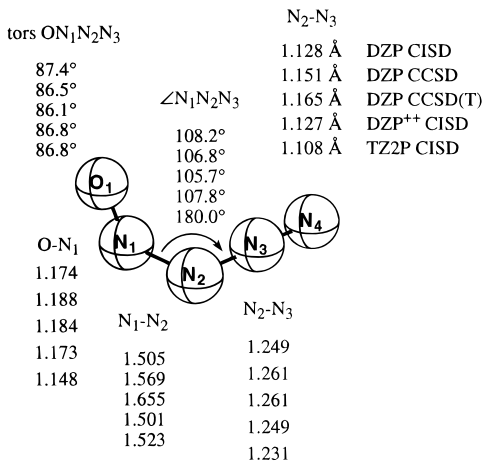

Figure 2. Predicted geometrical parameters for the C_1-symmetry ^1A *trans*-chain to *cis*-chain TS.

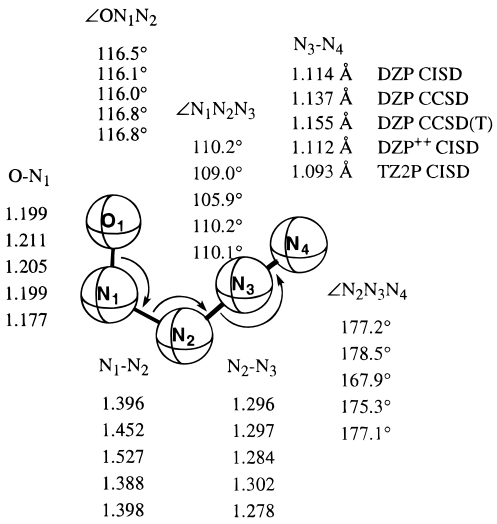

Figure 3. Predicted geometrical parameters for the C_s-symmetry $\tilde{X}\ ^1A'$ *cis*-chain isomer.

Force constants were determined only for the *trans*-chain structure and the ring structure, as these were decided to be the most likely targets for future experimental work. Force constants were also determined for the dissociation products N_2 and N_2O for comparative purposes.

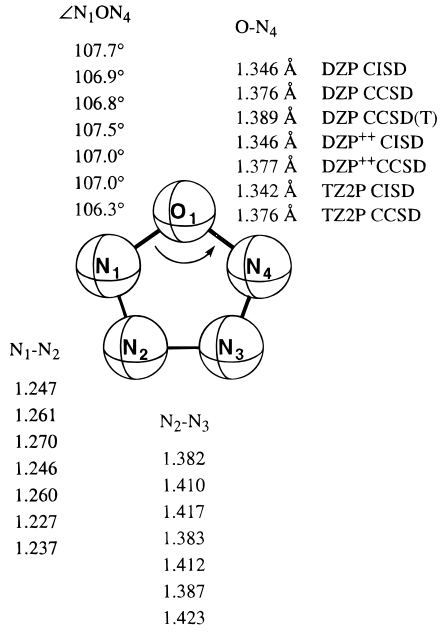

Figure 4. Predicted geometrical parameters for the C_{2v}-symmetry $\tilde{X}\ ^1A_1$ ring isomer.

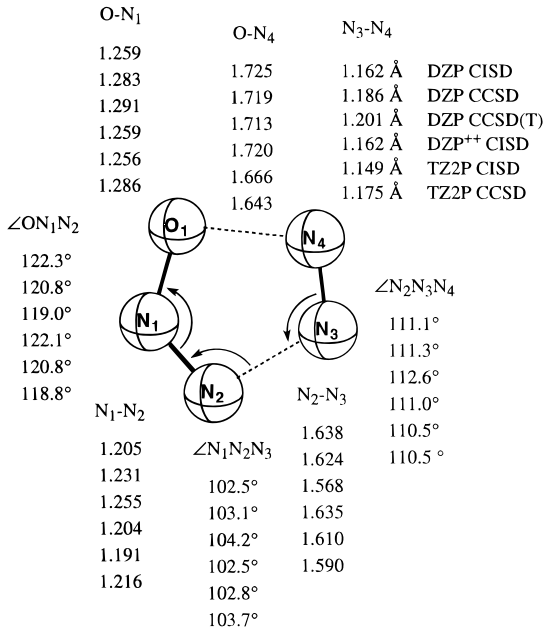

Figure 5. Predicted geometrical parameters for the C_s-symmetry $^1A'$ ring dissociation TS.

In discussing the N_4O PES, all molecular orbital (MO) arguments are based on CINOs generated at the DZP CISD level of theory. Mulliken bond indices[35] (MBI) have also been used in order to aid in describing bonding among various isomers. While the simplicity of the MBI is one of its greatest attributes, it has also been the source of much criticism.[36] The use of MBI is justified in the present study for comparing similar structures. The shortcomings of these methods will

(34) Pople, J. A.; Raghavachari, K.; Schlegel, H. B.; Binkley, J. S. *Int. J. Quantum Chem*. **1979**, *S 13*, 225. Saxe, P.; Yamaguchi, Y.; Schaefer, H. F. *J. Chem. Phys*. **1982**, *77*, 5647. Osamura, Y.; Yamaguchi, Y.; Saxe, P.; Vincent, M. A.; Gaw, J. F.; Schaefer, H. F. *Chem. Phys*. **1982**, *72*, 131. Osamura, Y.; Yamaguchi, Y.; Saxe, P.; Fox, D. J.; Vincent, M. A.; Schaefer, H. F. *J. Mol. Struct*. **1983**, *103*, 183.

(35) Mayer, I. *Chem. Phys. Lett*. **1983**, *97*, 270. Mayer, I. *Chem. Phys. Lett*. **1985**, *111*, 396. Mayer, I. *Int. J. Quantum Chem*. **1986**, *29*, 73. Based on the population analysis method of Mulliken: Mulliken, R. S. *J. Chem. Phys*. **1955**, *23*, 1833, 1841.

(36) Baker, J. *Theor. Chim. Acta* **1984**, *110*, 440. Reed, A. E.; Schleyer, P. v. R. *J. Am. Chem. Soc*. **1990**, *112*, 1434. Kar, T.; Behera, L.; Sannigrahi, A. B. *Chem. Phys. Lett*. **1989**, *163*, 157.

hopefully be reasonably consistent throughout all structures, giving a *qualitative* understanding of the entire hypersurface. As a result, emphasis will be placed on relative values as compared to other structures on the PES, as opposed to absolute values. In addition, no definite conclusions will be drawn from this method alone. All populations and bond indices were obtained at the DZP CISD level of theory in order to facilitate comparison with CINOs. All work was completed on IBM RS6000 workstations using the PSI 2.0.8 suite of programs.[37]

III. Results and Discussion

In the following discussion, all electronic structures are described in terms of symmetry orbitals as defined by Cotton.[38] In each case [core] denotes the 1s atomic orbitals (on each atom), which were not allowed to participate in correlated procedures. Initial characterization of states proceeded at the DZP SCF level of theory.

The first structures considered were the linear $C_{\infty v}$-symmetry $^3\Sigma^-$ and $^1\Delta$ states with electronic configuration

$$(^3\Sigma^-)\ [\text{core}]\ (6\sigma)^2(7\sigma)^2(8\sigma)^2(9\sigma)^2(10\sigma)^2(1\pi)^4 \times (11\sigma)^2(12\sigma)^2(2\pi)^4(3\pi)^4(4\pi)^2 \quad (2)$$

$$(^1\Delta)\ [\text{core}]\ (6\sigma)^2(7\sigma)^2(8\sigma)^2(9\sigma)^2(10\sigma)^2(1\pi)^4 \times (11\sigma)^2(12\sigma)^2(2\pi)^4(3\pi)^4(4\pi)^2 \quad (3)$$

For computational expediency, these structures were considered in C_{2v} symmetry.

As expected, the linear $^3\Sigma^-$ state was 18.5 kcal mol^{-1} lower in energy. The vibrational frequency analysis of the corresponding stationary point determined this structure to be a higher order stationary point with imaginary modes corresponding to symmetry-lowering bending motions. Relaxing the symmetry restraints led to a C_s-symmetry stable minimum 77.7 kcal mol^{-1} lower in energy than the $^3\Sigma^-$ state:

$$(^3\text{A}'')\ [\text{core}]\ (6\text{a}')^2(7\text{a}')^2(8\text{a}')^2(9\text{a}')^2(10\text{a}')^2(11\text{a}')^2(1\text{a}'')^2 \times (12\text{a}')^2(2\text{a}'')^2(13\text{a}')^2(14\text{a}')^2(3\text{a}'')^2(15\text{a}')(4\text{a}'') \quad (4)$$

Further exploration of the triplet hypersurfaces at the DZP SCF level of theory revealed that 9.6 kcal mol^{-1} lower in energy than the ^{3}A″ state is the ^{3}A′ state:

$$(^3\text{A}')\ [\text{core}]\ (6\text{a}')^2(7\text{a}')^2(8\text{a}')^2(9\text{a}')^2(10\text{a}')^2(11\text{a}')^2(1\text{a}'')^2 \times (12\text{a}')^2(2\text{a}'')^2(13\text{a}')^2(14\text{a}')^2(3\text{a}'')^2(15\text{a}')(16\text{a}') \quad (5)$$

The singlet states were also investigated, starting with the linear $^1\Delta$ state discussed above. This state was also determined to be a higher order stationary point. Following the above procedure for the triplets, two other singlet structures were found.

$$(^1\text{A}')\ [\text{core}]\ (6\text{a}')^2(7\text{a}')^2(8\text{a}')^2(9\text{a}')^2(10\text{a}')^2(1\text{a}'')^2 \times (11\text{a}')^2(12\text{a}')^2(2\text{a}'')^2(13\text{a}')^2(14\text{a}')^2(3\text{a}'')^2(4\text{a}'')^2 \quad (6)$$

$$(^1\text{A}')\ [\text{core}]\ (6\text{a}')^2(7\text{a}')^2(8\text{a}')^2(9\text{a}')^2(10\text{a}')^2(11\text{a}')^2 \times (1\text{a}'')^2(12\text{a}')^2(13\text{a}')^2(2\text{a}'')^2(14\text{a}')^2(3\text{a}'')^2(15\text{a}')^2 \quad (7)$$

The state with the 4a″ highest occupied molecular orbital (HOMO) was 123 kcal mol^{-1} higher in energy and was found to be unstable with respect to out-of-plane bending. When the HOMO is the 15a′, however, the energy drops to 18.2 kcal mol^{-1} below that of the lowest triplet state of N_4O. In order to make sure that this *trans*-chain ^{1}A′ state was the ground state, CCSD(T) energy points for the ^{1}A′, ^{3}A′, and ^{3}A″ states were determined at the DZP CISD optimized geometry. All energy relationships remained qualitatively the same, making the *trans*-chain ^{1}A′ state the uncontested open-chain ground state by a 30.6 kcal mol^{-1} margin. This structure is represented in Figure 1.

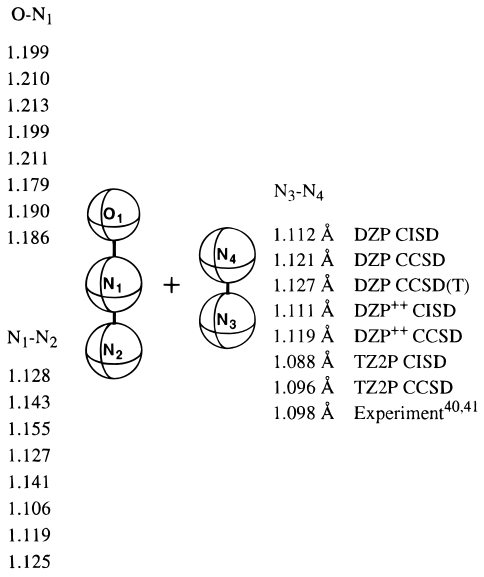

Figure 6. Predicted geometrical parameters for the N_4O dissociation products $\tilde{X}\ ^1\Sigma_g^+$ N_2 and $\tilde{X}\ ^1\Sigma^+$ N_2O.

Exploration of the PES led to a C_1-symmetry transition state (TS) (Figure 2) between the *trans*-chain isomer and the C_s-symmetry *cis*-chain (Figure 3) structure with electronic configuration

$$(^1\text{A}')\ [\text{core}]\ (6\text{a}')^2(7\text{a}')^2(8\text{a}')^2(9\text{a}')^2(10\text{a}')^2(11\text{a}')^2 \times (1\text{a}'')^2(12\text{a}')^2(13\text{a}')^2(2\text{a}'')^2(14\text{a}')^2(15\text{a}')^2(3\text{a}'')^2 \quad (8)$$

The only difference between electronic configurations 7 (*trans*) and 8 (*cis*) is the energetic ordering of the last two MOs. The (^{1}A) electronic structure of the C_1-symmetry TS (Figure 2) is trivial as all orbitals are of the same (a) symmetry. Further investigation led to theC_{2v}-symmetry ring structure (Figure 4, eq 11) and a C_s-symmetry TS (Figure 5, eq 12) to the dissociation products N_2 and N_2O (Figure 6).

$$(^1\text{A}_1)\ [\text{core}]\ (4\text{a}_1)^2(5\text{a}_1)^2(3\text{b}_2)^2(4\text{b}_2)^2(6\text{a}_1)^2(7\text{a}_1)^2 \times (1\text{b}_1)^2(8\text{a}_1)^2(5\text{b}_2)^2(2\text{b}_1)^2(6\text{b}_2)^2(9\text{a}_1)^2(1\text{a}_2)^2 \quad (9)$$

$$(^1\text{A}')\ [\text{core}]\ (6\text{a}')^2(7\text{a}')^2(8\text{a}')^2(9\text{a}')^2(10\text{a}')^2(11\text{a}')^2 \times (1\text{a}'')^2(12\text{a}')^2(13\text{a}')^2(2\text{a}'')^2(14\text{a}')^2(3\text{a}'')^2(15\text{a}')^2 \quad (10)$$

The dissociation products N_2 and N_2O are defined by the linear point groups $D_{\infty h}$ and $C_{\infty v}$, respectively:

$$(\text{N}_2)\ (^1\Sigma_g^+)\ [\text{core}]\ (3\sigma_g)^2(4\sigma_g)^2(1\sigma_u)^2(1\pi_u)^4 \quad (11)$$

$$(\text{N}_2\text{O})(^1\Sigma^+)\ [\text{core}]\ (4\sigma)^2(5\sigma)^2(6\sigma)^2(7\sigma)^2(1\pi_u)^4(2\pi_u)^4 \quad (12)$$

For computational expediency, these two species were consid-

(37) Janssen, C. L.; Seidl, E. T.; Scuseria, G. E.; Hamilton, T. P.; Yamaguchi, Y.; Remington, R. B.; Xie, Y.; Vacek, G.; Sherrill, C. D.; Crawford, T. D.; Fermann, J. T.; Allen, W. D.; Brooks, B. R.; Fitzgerald, G. B.; Fox, D. J.; Gaw, J. F.; Handy, N. C.; Laidig, W. D.; Lee, T. J.; Pitzer, R. M.; Rice, J. E.; Saxe, P.; Scheiner, A. C.; Schaefer, H. F. *PSI 2.0.8*; PSITECH Inc.: Watkinsville, GA, 1994.

(38) Cotton, F. A. *Chemical Applications of Group Theory*, 3rd ed.; John Wiley and Sons: New York, 1990.

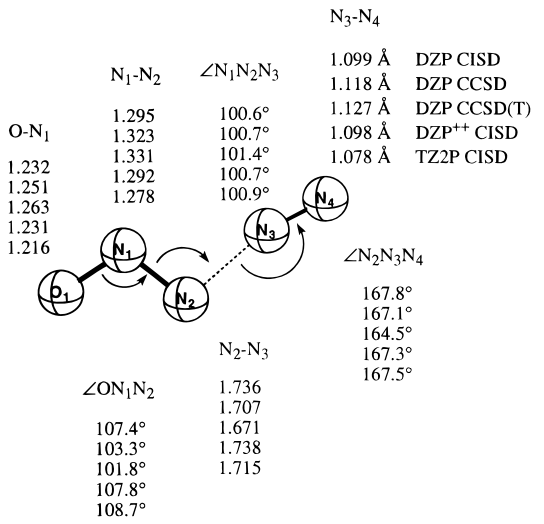

Figure 7. Predicted geometrical parameters for the C_s-symmetry $^1A'$ *trans*-chain to $N_2 + N_2O$ TS.

ered in C_{2v} symmetry:

$$(N_2)\ (^1A_1)\ [\text{core}]\ (3a_1)^2(4a_1)^2(5a_1)^2(1b_1)^2(1b_2)^2 \quad (13)$$

$$(N_2O)\ (^1A_1)\ [\text{core}]\ (4a_1)^2(5a_1)^2(6a_1)^2(7a_1)^2(5a_1)^2 \times (1b_1)^2(1b_2)^2(2b_1)^2(2b_2)^2 \quad (14)$$

Lastly, in an effort to determine the direct dissociation pathway of the *trans*-chain isomer, a C_s-symmetry TS was found after elongation of the N_2-N_3 bond (Figure 7):

$$(^1A')\ [\text{core}]\ (6a')^2(7a')^2(8a')^2(9a')^2(10a')^2(11a')^2 \times (12a')^2(1a'')^2(13a')^2(2a'')^2(14a')^2(3a'')^2(15a')^2 \quad (15)$$

Geometrical Parameters and Vibrational Frequencies: *Trans*-Chain Isomer. The geometric parameters for the $\tilde{X}\ ^1A'$ *trans*-chain state of N_4O are represented in Figure 1. Thomas, DeLeeuw, Vacek, Crawford, Yamaguchi, and Scheafer[39] have determined that a proper "balance" between theoretical method and basis set size can be achieved with CCSD in conjunction with a TZ2P basis set. At this level of theory, Thomas *et al*. found the predicted equilibrium bond lengths of a variety of small molecules to be merely 0.15% in error vis-à-vis experimentally determined bond lengths. The only other combination which leads to comparable results was found to be a TZ2P basis set with the inclusion of higher angular momentum f-type functions (TZ2P+f) along with CCSD(T). In the present study, TZ2P+f CCSD(T) was deemed prohibitively computation intensive. As a result, the TZ2P CCSD predictions reported in Figure 1 are our best results.

Comparing our TZ2P CCSD predictions for the $O-N_1$ bond with experimentally determined bond lengths of some similar molecules (there are no experimental results for N_4O itself), we see that the predicted N−O bond of N_4O (1.177 Å) lies between the diatomic NO (1.151 Å)[40] and N_2O (1.186 Å)[41] N−O bond lengths, favoring N_2O slightly. Comparison to the N−O bond length in N_2O predicted at the same levels of theory (Figure 6) shows the N−O bond length in N_4O to be shorter by 0.010 ± 0.003 Å. As a result the true N−O bond distance in N_4O is expected to be near 1.176 ± 0.003 Å. This is in agreement with trends developed in improving basis set size and correlation scheme; basis set improvements shorten the bond length while more complete correlation schemes increase the bond length.

A comparison of any of the predicted N_1-N_2 bond lengths for N_4O with the predicted or experimental (1.127 Å)[41] N_2O nitrogen−nitrogen bond lengths shows that the N_1-N_2 bond is definitely longer than the nitrogen−nitrogen bond in N_2O. The TZ2P CCSD prediction (1.472 Å) is our best estimate for the N_1-N_2 bond distance in N_4O. This prediction is longer than the experimental nitrogen−nitrogen bond length in hydrazine, N_2H_4 (1.449 Å),[42] but much shorter than the nitrogen−nitrogen bond length in the weakly bound dinitrogen tetraoxide, N_2O_4 (1.782 Å).[43]

The predicted N_2-N_3 and N_3-N_4 bond lengths are very similar to experimental[44] and theoretical[45] bond distances for the halogen azides, XN_3 (X = H, F, Cl, Br, I). As there are no clear trends upon improving basis set size or correlation scheme, the predicted TZ2P CCSD N_2-N_3 bond length (1.272 Å) is our best estimate for the N_2-N_3 bond distance in N_4O.

The predicted TZ2P CCSD N_3-N_4 bond length, on the other hand, is shorter than all XN_2-N bond lengths (except IN_3) by at most 0.016 Å. In this case improvements in theoretical method and basis set follow more regular trends. Assuming a similar increase from TZ2P CCSD to CCSD(T) as with DZP CCSD to CCSD(T) yields 1.130 Å with improvements toward the basis set limit lowering the bond length even more.

The theoretically predicted harmonic vibrational frequencies and IR intensities of the N_4O *trans*-chain isomer are presented in Table 1. Table 2 includes harmonic vibrational frequencies for N_2 and N_2O for comparative purposes. Figure 8 is a pictorial representation of the N_4O *trans*-chain normal modes. As with the equilibrium bond lengths and angles, Thomas *et al*.[39] found a good "balance" between basis set size and level of theory for harmonic vibrational predictions with the TZ2P CCSD theoretical method. While Thomas *et al*. found predictions at this level to be in error by only 1.5% in comparison to experimental *harmonic* vibrational frequencies, valid comparisons can still be made to the *fundamental* vibrational frequencies of Schultz *et al*.[6] if the lowering of fundamental vibrations due to anharmonic effects is taken into account.

Figure 8 shows the ω_1 to be almost purely an N−N stretching vibration of the terminal nitrogens. The TZ2P CCSD value, 2217 cm^{-1}, is slightly above the experimental value, 2207 cm^{-1}, as expected. Upon inclusion of triple excitations with a DZP basis, this prediction drops to 2104 cm1$-^1$. Basis set trends established with CISD and CCSD, however, indicate that increasing the basis set size with CCSD(T) will increase this frequency to a more satisfactory level.

Figure 8 shows ω_2 to be almost purely an O−N stretch. Although the TZ2P CCSD value, 1691 cm^{-1}, is our highest level prediction, estimates to higher levels indicates that improvements in basis set size will decrease the DZP CCSD-

(39) Thomas, J. R.; DeLeeuw, B. J.; Vacek, G.; Crawford, T. D.; Yamaguchi, Y.; Schaefer, H. F. *J. Chem. Phys*. **1993**, *99*, 403.
(40) Huber, K. P.; Herzberg, G. *Constants of Diatomic Molecules*; Van Nonstrand Reinhold: New York, 1979.
(41) Herzberg, G. *Electronic Spectra and Electronic Structure of Polyatomic Molecules*; Krieger: Malabar, 1991.
(42) Kuhata, K.; Fukuyama, T.; Kuchitsu, K. *J. Phys. Chem*. **1982**, *86*, 602.
(43) McClelland, B. W.; Gundersen, G.; Hedberg, K. *J. Chem. Phys*. **1972**, *56*, 4541.
(44) (a) HN_3: Winnewisser, B. P. *J. Mol. Spectrosc*. **1980**, *82*, 220. (b) FN_3: Chisten, D.; Mack, H. G.; Schatte, G.; Willner, H. *J. Am. Chem. Soc*. **1988**, *110*, 707. (c) ClN_3: Cook, R. L.; Gerry, M. C. L. *J. Chem. Phys*. **1970**, *53*, 2525. (d) BrN_3: Hargittai, M.; Tornieporth-Oetting, I. C.; Klapötke, T. M.; Kolonits, M.; Hargittai, I. *Angew. Chem., Int. Ed. Engl*. **1993**, *32*, 759. (e) IN_3: Buzek, P.; Klapötke, T. M.; Schleyer, P. v. R.; Tornieporth-Oetting, I. C.; White, P. S. *Angew. Chem., Int. Ed. Engl*. **1993**, *32*, 275.
(45) Otto, M.; Lotz, S. D.; Frenking, G. *Inorg. Chem*. **1992**, *31*, 3647. Also refs 44d,e.

Table 1. Correlated Theoretical Predictions for the Harmonic Vibrational Frequencies (and Infrared Intensities) of the $\tilde{X}\ ^1A'$ N_4O *trans*-Chain Isomer[a]

method	$\omega_1(a')$	$\omega_2(a')$	$\omega_3(a')$	$\omega_4(a')$	$\omega_5(a')$	$\omega_6(a')$	$\omega_7(a')$	$\omega_8(a'')$	$\omega_9(a'')$
DZP CISD	2385 (477)	1816 (316)	1151 (93)	1009 (692)	638 (32)	616 (53)	227 (2)	605 (6)	194 (1)
DZP^{++} CISD	2389 (469)	1812 (333)	1144 (87)	1014 (734)	646 (33)	619 (45)	231 (2)	583 (7)	182 (1)
TZ2P CISD	2407 (483)	1809 (319)	1149 (123)	953 (646)	638 (2)	616 (145)	228 (2)	599 (7)	195 (1)
DZP CCSD	2194 (455)	1693 (283)	1104 (143)	895 (508)	582 (1)	551 (146)	206 (1)	562 (0)	174 (0)
DZP^{++} CCSD	2199 (447)	1688 (295)	1092 (132)	899 (562)	585 (0)	562 (135)	210 (2)	771 (5)	332 (0)
TZ2P CCSD	2217 (463)	1691 (314)	1098 (161)	845 (450)	590 (5)	513 (239)	204 (3)	549 (5)	174 (0)
DZP CCSD(T)	2104 (440)	1638 (349)	1115 (174)	827 (358)	564 (7)	465 (253)	191 (2)	544 (4)	166 (0)
MP2/6-31+G* [b]	2312 (2208)	1568 (1498)	1158 (1106)	818 (780)	606 (579)	416 (397)	189 (180)	506 (493)	168 (160)
expt[b]	2207	1485	1095	784	566	415		484	162

[a] Harmonic vibrational frequencies are in cm^{-1}, and infrared intensities are in km mol^{-1}. Frequency lables refer to Figure 8. [b] MP2/6-31+G* predictions (scaled by 0.955) and experimental fundamental Raman frequencies from A. Schultz *et al*. (ref 6).

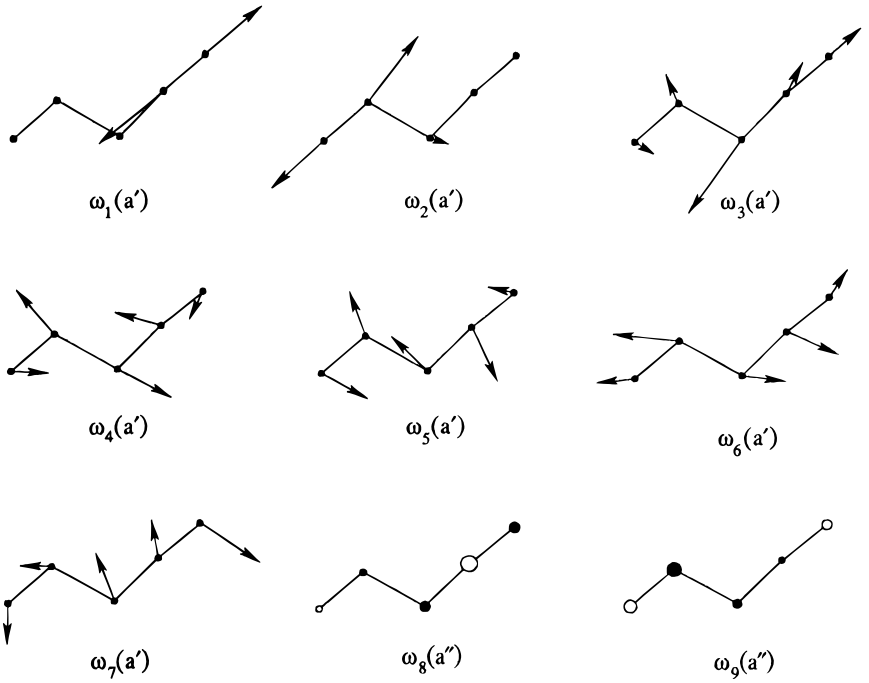

Figure 8. Normal modes of vibration for the C_s-symmetry $\tilde{X}\ ^1A'$ *trans*-chain isomer predicted at the TZ2P CCSD level of theory.

Table 2. Correlated Theoretical Predictions for the Harmonic Vibrational Stretching Frequencies of $\tilde{X}\ ^1\Sigma_g^+$ N_2 and $\tilde{X}\ ^1\Sigma^+$ N_2O[a]

	N_2	N_2O	
method	N−N str	N−O str	N−N str
DZP CISD	2444	1352	2402
DZP^{++} CISD	2452	1345	2400
TZ2P CISD	2500	1354	2417
DZP CCSD	2352	1290	2296
DZP^{++} CCSD	2361	1281	2292
TZ2P CCSD	2414	1288	2307
DZP CCSD(T)	2287	1269	2222
expt[b]	2359.6	1284.9	2223.76

[a] Harmonic vibrational frequencies are in cm^{-1}. [b] Experimental N_2 harmonic frequency from ref 40. N_2O fundamentals from ref 41.

(T) predicted value, 1638 cm^{-1}. The experimental value of Schultz *et al*.,[6] 1485 cm^{-1}, is well below this value even with a modest decrease from 1638 cm^{-1}, indicating perhaps a high degree of anharmonicity in this mode.

The assignment of ω_3 is not as straightforward as with ω_1 and ω_2, illustrating the utility of Figure 8. The ω_3 motion pictorially represented in Figure 8 can be described as a mixture of N_2-N_3 and N_3-N_4 stretching along with $O-N_1-N_2$ bending. The TZ2P CCSD predicted harmonic frequency, 1098 cm^{-1}, is most similar to the symmetric stretching frequencies of the halogen azides (1168, 1090, 1134, 1160, and 1207 cm^{-1} for HN_3,[46] FN_3,[47] ClN_3,[48] BrN_3,[49] and IN_3,[50] respectively). The TZ2P CCSD predicted ω_3 is in good agreement with the experimental Raman ν_3 fundamental of Schultz *et al*.[6] (1095 cm^{-1}).

As seen in Figure 8, both of the ω_4 and ω_5 modes can be described as a mixture of stretching and bending modes. The TZ2P CCSD values for ω_4 and ω_5 (845 and 590 cm^{-1}, respectively) are higher than the ν_4 and ν_5 Raman adsorbances of Schultz *et al*.[6] (784 and 566 cm^{-1}), as is expected. Extension to CCSD(T) with a larger basis set is expected to lower the ω_4 mode from the DZP CCSD(T) value of 827 cm^{-1} and raise the ω_5 mode from 564 cm^{-1}, in accordance with experimental observation.

Figure 8 indicates that ω_6 is most closely associated with a stretching of the N_1-N_2 bond in conjunction with some mixing of the $O-N_1-N_2$ bend. The TZ2P CCSD ω_6 frequency lies slightly below the M−NO stretching region in nitrosyl com-

(46) Winnewisser, B. P. *J. Mol. Spectrosc.* **1980**, *82*, 220.
(47) Moore, C. B.; Rosengreen, K. J. *J. Chem. Phys.* **1964**, *40*, 2461.
(48) Foy, B. R.; Casassa, M. P.; Stephenson, J. C.; King, D. S. *J. Phys. Chem.* **1979**, *83*, 429.
(49) Kajimoto, O.; Yamamoto, T.; Fueno, T. *J. Phys. Chem.* **1979**, *83*, 429.
(50) Richardson, W. C.; Setser, D. W. *Can. J. Chem.* **1969**, *47*, 2725.

Table 3. Correlated Theoretical Predictions for the Harmonic Vibrational Frequencies (and Infrared Intensities) of the $\tilde{X}\ ^1A_1$ N_4O Ring Isomer[a]

method	$\omega_1(a_1)$	$\omega_2(a_1)$	$\omega_3(a_1)$	$\omega_4(a_1)$	$\omega_5(a_2)$	$\omega_6(b_1)$	$\omega_7(b_2)$	$\omega_8(b_2)$	$\omega_9(b_2)$
DZP CISD	1549 (15)	1189 (3)	1124 (16)	955 (47)	768 (0)	722 (0)	1654 (0)	1126 (1)	942 (10)
DZP^{++} CISD	1551 (16)	1186 (10)	1123 (22)	949 (26)	758 (0)	714 (0)	1655 (0)	1124 (1)	937 (11)
TZ2P CISD	1556 (13)	1173 (0)	1105 (20)	872 (43)	776 (0)	729 (0)	1656 (0)	1141 (1)	851 (10)
DZP CCSD	1460 (14)	1096 (0)	1028 (17)	844 (40)	720 (0)	676 (0)	1551 (0)	1061 (1)	779 (10)
DZP^{++} CCSD	1461 (15)	1092 (2)	1025 (27)	834 (23)	743 (0)	920 (0)	1712 (0)	1147 (0)	1047 (11)
TZ2P CCSD	1472 (13)	1093 (0)	984 (32)	735 (18)	724 (0)	679 (0)	1557 (0)	1071 (1)	661 (10)
DZP CCSD(T)	1389 (13)	1060 (0)	978 (16)	798 (36)	703 (0)	662 (0)	1477 (1)	1036 (1)	660 (8)
MP2/6-31+G* [b]	1248	1058	980	814	708	686	1330	1054	671

[a] Harmonic vibrational frequencies are in cm^{-1}, and infrared intensities are in km mol^{-1}. Frequency labels refer to Figure 9. [b] MP2/6-31+G* predictions from A. Schultz *et al*. (ref 6).

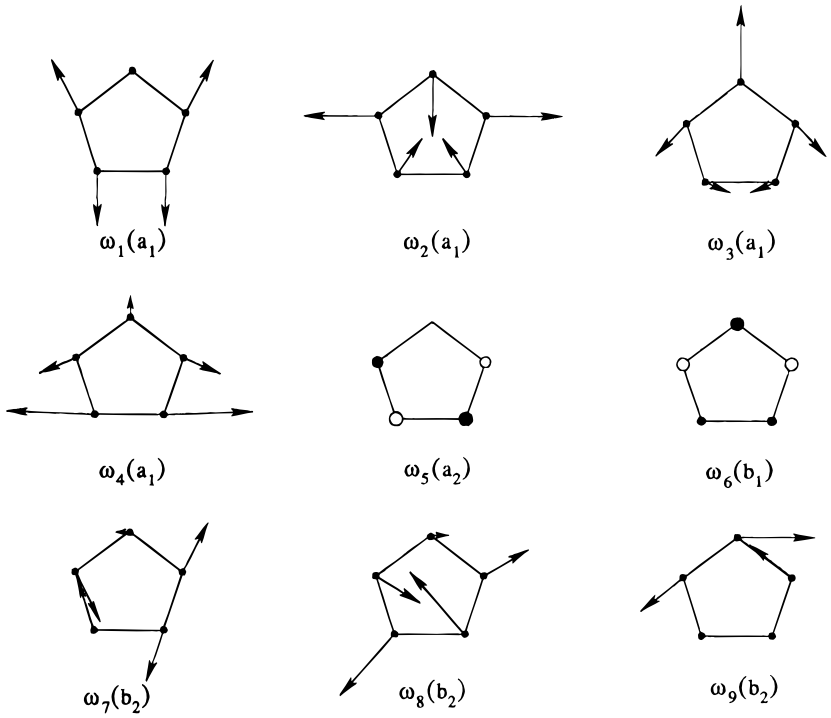

Figure 9. Normal modes of vibration for C_{2v}-symmetry $\tilde{X}\ ^1A_1$ ring isomer predicted at the TZ2P CCSD level of theory.

pounds (650−520 cm^{-1}).[51] Comparison with the results of Schultz *et al*. for ν_6 places the TZ2P CCSD prediction above the experimental frequency as expected; however, the lack of clear trends makes extension to larger basis set and higher level of theory inappropriate. As is evident from Table 1, ω_6 is the only mode for which there is a significant difference between our TZ2P CCSD predictions and the MP2/6-31+G* predictions of Schultz *et al*.

Schultz *et al*. did not observe a ν_7 frequency. The TZ2P CCSD prediction for the ω_7 stretch/bend at 204 cm^{-1} is our best estimate. While the TZ2P CCSD(T) prediction is expected to be lower on the basis of comparison of CISD and CCSD predictions, the effect of f-type functions is unclear.

While the predictions for the out-of-plane models, ω_8 and ω_9 (549 and 174 cm^{-1}), are completely reasonable when compared to the experimental Raman frequencies (484 and 162 cm^{-1}), a lack of clear trends in basis set extension makes any further estimate inappropriate.

Ring Isomer. When considering the geometrical parameters of the ring isomer, comparisons to N_2O and N_2 are inappropriate. Figure 4 shows that increasing the basis set size has a small effect on the O−N bond length. Therefore, extending the DZP CCSD(T) result to a larger basis set gives a final prediction of less than 1.389 Å. While longer than the O−N bond in many nitrogen oxides, this prediction is less than the O−N bridging bond in dinitrogen pentaoxide, $O_2N-O-NO_2$ (1.498 Å).[52] Basis set size, however, has an appreciable effect on the N_1-N_2 bond length, decreasing it by ∼0.02 Å upon moving from a DZP to a TZ2P basis (the effect of adding diffuse functions is negligible). As a result, the true bond length can be expected to be less than 1.250 Å (0.02 Å less than the DZP CCSD(T) with further reduction expected upon inclusion of f-type functions), placing this bond length near that of diimide, N_2H_2 (1.252 Å).[53] Conversely, the N_2-N_3 bond length increases with larger basis sets as well as improved correlation schemes. The amount of increase, however, is not steady so that we can only be sure that N_3-N_4 will be >1.423 Å (predicted at TZ2P CCSD). All predicted bond angles are constant with respect to theoretical method to less than a degree.

The predicted vibrational frequencies and IR intensities of the ring isomer are displayed in Table 3, and a pictorial representation of the normal modes is given in Figure 9. The symmetric stretching of N_1-N_2 and N_3-N_4 (ω_1) drops 71 cm^{-1} in going from CCSD to CCSD(T) with a DZP basis set whereas

(51) Socrates, G. *Infrared Characteristic Group Frequencies*, 2nd ed.; John Wiley and Sons: New York, 1994.

(52) McClelland, B.; Hedberg, L.; Hedberg, K.; Hagen, K. *J. Am. Chem. Soc.* **1983**, *105*, 3789.

(53) Carlotti, N.; Johns, J. W. C.; Tromeetti, A. *Can. J. Phys.* **1974**, *52*, 340.

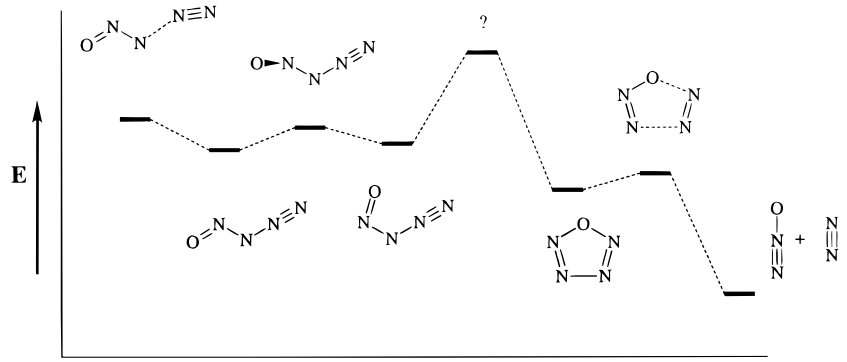

Figure 10. Qualitative description of the entire N_4O potential energy hypersurface. "?" indicates that no stationary point has been found.

increasing the size of the basis set from DZP to TZ2P increases the frequency by 12 cm^{-1} at most (with CCSD). With this in mind and starting from the DZP CCSD(T) frequency at 1389 cm^{-1}, we expect the actual harmonic vibrational frequency to be above 1400 cm^{-1}. This is quite different from the lower level theoretical prediction of Schultz *et al.*[6] (1248 cm^{-1}).

The ω_2 ring flattening mode, the ω_3 O−N symmetric stretch, and the ω_4 N_2−N_3 stretch, however, decrease with both basis set size and level of correlation. As a result, the true harmonic vibrational frequency is expected to be les than the DZP CCSD-(T) predictions of 1060, 978, and 798 cm^{-1}, respectively. Agreement with the predictions of Schultz *et al.*[6] is much better in this case (1058, 980, and 814 cm^{-1}, respectively).

The TZ2P CCSD predictions for the out-of-plane modes (724 and 679 cm^{-1} for ω_5 and ω_6, respectively) must be considered our best values, as confident estimates to higher level of theory cannot be made. These predictions are in reasonable agreement with the predictions of Schultz *et al.*[6] (708 and 686 cm^{-1}, respectively). Similarly, higher level of theory estimates cannot be made for the asymmetric N−N stretch, ω_7, the asymmetric ring deformation, ω_8, and the asymmetric O−N stretch, ω_9. The TZ2P CCSD predictions for ω_8 and ω_9 (1071 and 661 cm^{-1}, respectively) are in good agreement with the predictions of Schultz *et al.* (1054 and 671 cm^{-1}, respectively); however, their ω_7 (1330 cm^{-1}) is suspiciously below the TZ2P CCSD prediction (1557 cm^{-1}).

The N_4O Potential Energy Hypersurface. A qualitative description of the N_4O PES is shown in Figure 10. There are several possible ways of drawing reasonable Lewis structures for the N_4O *trans*-chain isomer, a few of which are represented below:

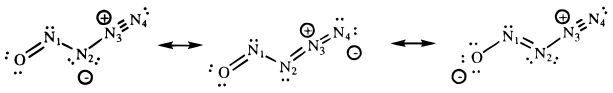

The MBI (Figure 11) indicate that the O−N_1 bond is between a single and a double bond, the N_2−N_3 bond is slightly more than a single bond, and the N_3−N_4 is less than a triple bond. Comparison with the MBI of N_2 and N_2O determined by the same computational procedure confirms these ideas. The bond index of the O−N_1 bond is greater than that of the N_2O N−O bond (which is generally considered to be slightly more than a single bond), while the MBI of the N_3−N_4 bond is less than that of the classic triple bond in N_2. This deviation from whole-number bond order is a result of the delocalized π system.

The same conclusions can be drawn by comparing the bond lengths and vibrational frequencies to those of known O−N and N−N single, double, and triple bonds. The O−N bond in N_4O is longer than the O−N double-bond length in NO[40] but shorter than the single bond in O_2N−O−NO_2 (1.498 Å).[52]

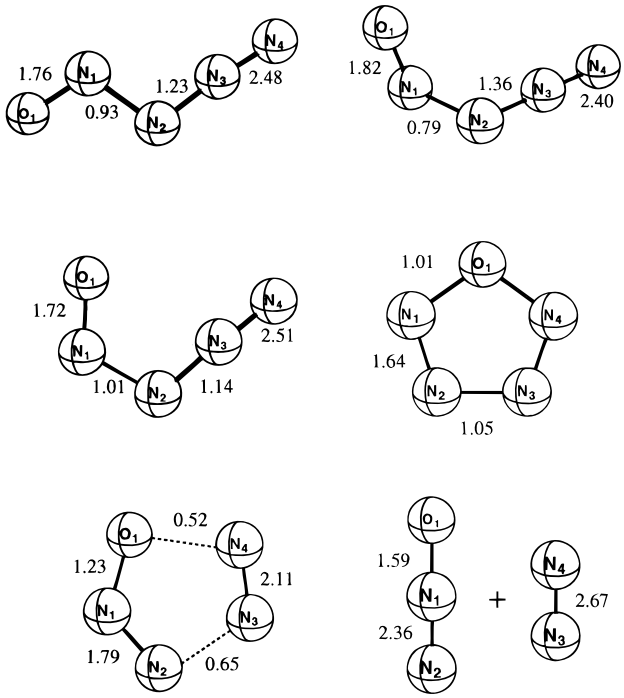

Figure 11. Mulliken bond indices of various stationary points on the N_4O potential energy surface predicted at the DZP CISD level of theory.

Similarly, comparison to known N−O stretching vibrations places N_4O between N_2O (1284.9 cm^{-1})[41] and NO (1904.2 $cm.^{-1}$).[40] The N_3−N_4 bond length in N_4O is longer than the N−N triple-bond length in N_2[40] but shorter than the double-bond length in N_2H_2.[53] Comparison to the N−N triple-, double-, and single-bond stretch in N_2[40] (2358.6), N_2H_2[54] (1529 cm^{-1}), and N_2H_4[55] (1087 cm^{-1}) places the N_4O N_3−N_4 stretch between the stretch of a N−N triple bond and a N−N double bond, but closer to the triple bond. Comparison with analogous N_2 theoretical results shows that the terminal N_3−N_4 bond becomes less like a classic N_2 triple bond with increased electron correlation. With CISD these values are ∼0.008 Å longer than the N_2 bond length while CCSD results are off by 0.018 Å and the DZP CCSD(T) bond length is greater by 0.025 Å. In addition the N_2−N_3 bond length lies between the single N−N bond length in N_2H_4[56] (1.447 Å) and the double N−N bond length in N_2H_2 (1.252 Å).[53]

Our first attempts to find a transition state (TS) between the *trans*- and *cis*-chain isomers involved increasing the O−N_1−N_2 angle while retaining C_s symmetry. All such attempts

(54) Bondybey, V. E.; Nibler, J. W. *J. Chem. Phys.* **1973**, *58*, 2125.
(55) Catalano, E.; Sanborn, R. H.; Frazer, J. W. *J. Chem. Phys.* **1963**, *38*, 2265.
(56) Kuhata, K.; Fukuyama, T.; Kuchitsu, K. *J. Phys. Chem.* **1982**, *86*, 602.

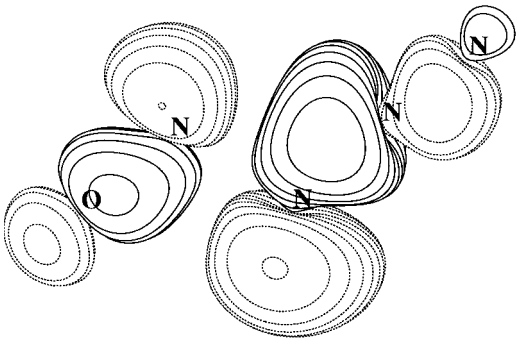

Figure 12. The 13a′ CI natural orbital of the C_s-symmetry $\tilde{X}\ ^1A'$ N_4O *trans*-chain isomer at the DZP CISD optimized geometry. $\angle ON_1N_2 = 110.6°$.

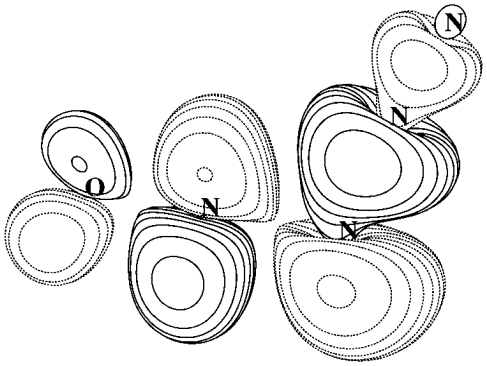

Figure 13. The 13a′ CI natural orbital of N_4O at $\angle ON_1N_2 = 180.0°$. All other geometrical parameters are held at the *trans*-chain DZP CISD optimized geometry.

resulted in failure, with the molecule dissociating into $N_2 + N_2O$. Upon releasing the symmetry restriction, a C_1-symmetry TS was easily found corresponding to rotation about the N_1-N_2 bond (Figure 2). The preference for a C_1-symmetry TS over a C_s-symmetry TS can be explained as an unfavorable energy change in moving from $O-N_1$ bond sp^2 hybridization in the *trans*-chain structure through sp hybridization and back to sp^2 hybridization in the *cis*-chain structure. This can be understood from a molecular orbital standpoint by following the 13a′ MO as the $O-N_1-N_2$ angle is increased. In the *trans*-chain structure, the 13a′ MO is largely $O-N_1$ bonding and N_1-N_2 antibonding (Figure 12). As the angle increases, the $O-N_1$ overlap becomes less favorable until at 180° (Figure 13) the 13a′ MO is $O-N_1$ as well as N_1-N_2 antibonding. Continuation along this path leads to $O-N_1$ and N_1-N_2 bonding interaction in the *cis*-structure (Figure 14). Rotation about the comparatively weak N_1-N_2 bond, however, is not accompanied by such an energetically unfavorable interaction.

Upon rotation about the N_1-N_2 bond, the $O-N_1$ π bond, which was delocalized over N_1 and N_2 in the *trans*-isomer, becomes more localized between O and N_1 as is evident by the decrease in the $O-N_1$ bond length and a subsequent increase in the N_1-N_2 bond length. Accordingly, the MBI increases between O and N_1 while decreasing between N_1 and N_2. On the other side of the molecule, the N_3-N_4 bond length increases as the N_2-N_3 bond length decreases, indicating a shift in electron density from the N_3-N_4 bond to a more delocalized $N_2-N_3-N_4$ π configuration. Rotation about the N_1-N_2 bond destroys the favorable overlap of the p-type orbital on N_2 with the p-type orbitals on O and N_1, thus making it available to accept electron density from the N_3-N_4 π system.

Energetically, the breaking of the extended π system by rotation about the N_1-N_2 bond is accompanied by a small energy barrier. As seen in Table 4, this energy barrier is no higher than ~13 kcal mol^{-1} and decreases with improvements in correlation scheme and basis set size. When corrected for ZPVE, this barrier drops even further. The C_1-symmetry MRCISD-A ZPVE corrected energy at the DZP CISD optimized geometry actually lies below the C_2-symmetry *trans*-chain isomer by 0.3 kcal mol^{-1}. Upon choosing a lower limit as the MRCISD cutoff (0.030), the energies returned to the expected ordering but with only a 4.1 kcal mol^{-1} energy difference. The barrier predicted with CCSD and CCSD(T) energy points, however, is ~10.0 kcal mol^{-1}, indicating that the number of reference configurations chosen may be insufficient.

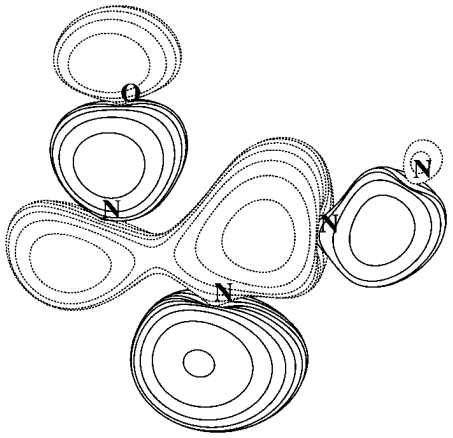

Figure 14. The 13a′ CI natural orbital of the C_s-symmetry $\tilde{X}\ ^1A'$ N_4O *cis*-chain isomer at the DZP CISD optimized geometry. $\angle ON_1N_2 = 116.5°$.

Further rotation to the *cis*-structure (Figure 3) results in an increase in the $O-N_1$ and N_2-N_3 bond lengths and a decrease in the N_1-N_2 and N_2-N_3 bond lengths. With the molecule once more contained in a single plane, delocalized π interaction over the entire molecule is again possible. The $O-N_1$ MBI decreases and the N_1-N_2 increases as the p-type orbital on N_2 becomes available to accept electron density from $O-N_1$. As a result, this p-type orbital is no longer exclusively involved in $N_2-N_3-N_4$ bonding and the MBI of N_2-N_3 decreases while the N_3-N_4 MBI increases.

With the π system spread across the entire molecule, the energy of the *cis*-chain isomer drops down near that of the *trans*-chain isomer and actually becomes lower in energy with MRCISD-A. When more references were included with the MRCISD-B method, the *cis*-chain isomer became 1.7 kcal mol^{-1} less stable than the *trans*-chain isomer (with ZPVE) while CCSD and CCSD(T) both predict barriers of ~1.0 kcal mol^{-1}, further illustrating the necessity for a higher number of references. This small *trans*/*cis*-chain energy difference is to be expected on the basis of steric hindrance arguments.

There remains an inconsistency between our *cis*-chain structure and the *cis*−*cis* structure of Klapötke *et al*.[9] A possible explanation of these results from a valence bond perspective has been provided by R. D. Harcourt.[57] The present conflict with *cis* N_4O may be similar to the case of N_2O_2, where Harcourt found two separate minima. The lower energy structure corresponds to a long, weak N−N bond made up of mostly p-type AOs. At higher energy, a second stable structure was found with an N−N bond length close to that of a single bond and involving more s-type character. From a molecular orbital standpoint, consideration of the molecule as a whole leads to the *cis*-chain structure found herein, whereas consideration of the NO and N_3 radicals as separate fragments leads to the *cis*−*cis* structure of Klapötke *et al*. It may be noted that the bond

(57) (a) Harcourt, R. D. *J. Mol. Struct. (THEOCHEM)* **1990**, *206*, 253. (b) Harcourt, R. D. *J. Mol. Struct. (THEOCHEM)* **1995**, *342*, 51.

Table 4. Energies[a] Relative to the Ring Isomer (ZPVE Corrected[b] in Parentheses) of Stationary Points on the N_4O Potential Energy Hypersurface

method	$N_2O + N_2$ TS	*trans*-chain	*trans*−*cis* TS	*cis*-chain	ring	ring-diss TS	$N_2O + N_2$
DZP CISD	36.5 (32.2)	20.9 (19.0)	33.8 (31.4)	21.6 (19.7)	0.0	15.3 (13.2)	−65.5 (−69.2)
DZP^{++} CISD	34.8 (30.5)	19.2 (17.3)	32.5 (30.1)	20.4 (18.5)	0.0	14.8 (12.7)	−66.8 (−70.5)
TZ2P CISD	29.6 (25.3)	13.8 (11.9)	26.0 (23.6)	14.8 (12.9)	0.0	10.1 (8.0)	−80.1 (−83.8)
DZP CCSD	34.7 (30.4)	19.9 (18.0)	30.8 (28.4)	20.7 (18.8)	0.0	8.7 (6.6)	−64.6 (−68.3)
DZP^{++} CCSD		18.3 (16.4)			0.0		−65.8 (−69.5)
TZ2P CCSD		13.2 (11.3)			0.0	4.4 (2.3)	−78.3 (−82.0)
DZP CCSD(T)	35.6 (31.3)	20.0 (18.1)	30.0 (27.6)	20.3 (18.4)	0.0	5.0 (2.9)	−61.9 (−65.6)
MRCISD-A[c]		19.6 (17.7)	19.8 (17.4)	19.3 (17.4)	0.0	11.0 (8.9)	
MRCISD-B[c]		19.8 (17.9)	24.4 (22.0)	21.5 (19.6)	0.0	5.2 (3.1)	
CCSD[c]		20.0 (18.1)	31.0 (28.6)	20.8 (18.9)	0.0	8.4 (6.3)	
CCSD(T)[c]		20.4 (18.5)	30.9 (28.5)	21.2 (19.3)	0.0	4.2 (2.1)	

[a] Energies in kcal mol^{-1}. [b] DZP CISD ZPVE corrections are used for all methods. [c] Energy at the DZP CISD optimized geometry.

lengths which we have calculated for the *cis*-chain structure (Figure 3) are in general accord with those that are implied by increased-valence structure (37) of ref 57b. All attempts to find a structure similar to the *cis*−*cis* structure resulted in failure.

Several failed attempts were made to find a TS between the *cis*-chain and ring isomers. At the SCF level, a TS seemed to have been found with the geometry of Figure 5. However, when electron correlation was considered, the energy of this structure dropped below that of all the open-chain isomers, indicating that the structure in Figure 5 is the ring dissociation TS and not the *cis*-chain cyclization TS.

One can draw the N_4O ring isomer (Figure 4) adhering to all the rules for a stable Lewis structure.

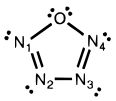

Considering the predicted bond lengths and MBI, this simple structure is not too far off the mark. The N_1-N_2/N_3-N_4 bonds (1.237 Å) are definitely shorter than the N_2-N_3 bond (1.423 Å). The bond orders of the $O-N_1/O-N_4$ and N_2-N_3 bonds are very nearly unity while the O−N bond length (1.376 Å) lies between the single (1.498 Å) and double (1.188 Å) O−N bond lengths in $O_2N-O-NO_2$,[52] favoring the single-bond length, and the N_2-N_3 bond lies closer to the singly bonded N_2H_4 (1.447 Å)[56] than the doubly bonded N_2H_2 (1.252 Å).[53] Furthermore, the N_1-N_2/N_3-N_4 bond lengths are close to the double-bond length in N_2H_2. In an ideal five-membered ring with 6 π electrons, the π electrons would be distributed evenly among all the bonds. In the present case, the highly electronegative O atom prefers to keep electrons around itself, leading to a partial negative charge on the oxygen. Energetically, there is a certain degree of stability associated with the ring isomer, although not on the order of common aromatic systems. The ring isomer is predicted to be at most (DZP CISD) 20.9 kcal mol^{-1} more stable than the *trans*-chain isomer; however, this value decreases to 13.2 kcal mol^{-1} with TZ2P CCSD.

The ring isomer TS to dissociation into N_2 and N_2O is shown in Figure 5. MBI show $O-N_1$ and N_1-N_2 increasing in bond order toward their values in the dissociation products while $O-N_4$ and N_2-N_3 decrease toward 0. Recently, Lendvay[58] has used MBI to define a "progress variable" χ_{AB} in order to characterize the development of a bond A−B as

$$\chi_{AB} = (B_{AB} - B_{AB}^{i})/(B_{AB}^{f} - B_{AB}^{i}) \qquad (16)$$

where B_{AB}^{i} and B_{AB}^{f} are the initial and final bond orders, respectively, and B_{AB} is the bond order at the point in question. Using this definition for the development of the $O-N_1$ and N_1-N_2 bond we arrive at 0.38 and 0.21, respectively. The same criterion can be applied to the $O-N_4$ and N_2-N_3 bond degradation, arriving at values of 0.48 and 0.38, respectively. Each of these sets of progress variables shows the TS to lie more toward the higher energy ring isomer, in agreement with Hammond's postulates.[59] Energetically, the barrier to dissociation is at most 15.3 kcal mol^{-1} (DZP CISD) and drops lower with improvements in both basis set and correlation scheme. In going from a DZP to a TZ2P basis set, for example, this barrier drops by 5.2 kcal mol^{-1} for CISD and 4.3 kcal mol^{-1} for CCSD. Assuming a similar trend in moving from DZP CCSD(T) to TZ2P CCSD(T), the ring dissociation barrier is expected to drop to 1−2 kcal mol^{-1} with the addition of f-type functions possibly making it even lower. A barrier of this size lies below the ZPVE, throwing doubt on the existence of the N_4O ring isomer.

Another possibility for the dissociation of the *trans*-chain isomer is the direct breaking of the N_2-N_3 bond (Figure 7). While the N_3-N_4 bond distance has decreased close to the diatomic N_2 bond length, the ON_1N_2 angle has gotten smaller and the $O-N_1$ bond length has increased past the linear N_2O N−O bond length, indicating that the structure in Figure 7 may be a TS to cyclic N_2O and N_2, as described by Tornieporth-Oetting *et al.*[10] Energetically, this barrier remains at ∼13.0 kcal mol^{-1} and is relatively insensitive to improvements in basis set size or treatment of electron correlation.

IV. Conclusions

The N_4O singlet potential energy hypersurface has been studied in detail using *ab initio* techniques. While the $^1A'$ *trans*-chain structure is the lowest energy open chain isomer, facile transformation into the slightly less stable (∼1 kcal mol^{-1}) *cis*-chain structure is expected to occur via a C_1-symmetry TS 9.5 kcal mol^{-1} (including ZPVE) above the *trans*-chain isomer. The ring structure was found to be 11.3 kcal mol^{-1} (including ZPVE) more stable than the *trans*-chain isomer. Although the addition of diffuse functions do not change this energy appreciably, extension to the TZ2P basis set significantly lowers the energy of the *trans*-chain isomer relative to the ring isomer. While improving the treatment of correlation from CISD to CCSD also lowers the relative energy, inclusion of triple excitations via the CCSD(T) method increases this energy difference by a

(58) Lendvay, G. *J. Phys. Chem.* **1994**, *98*, 6098.

(59) Hammond, G. S. *J. Am. Chem. Soc.* **1995**, *77*, 334.

mere 0.1 kcal mol^{-1}. As a result the *trans*-chain/ring energy difference can be expected[60] to be ~13.3 kcal mol^{-1}.

The geometrical parameters and vibrational frequencies of the *trans*-chain isomer have been characterized for a variety of theoretical methods in reasonable agreement with the previous experimental work of Schultz *et al*.[6] In addition, the geometrical parameters and vibrational frequencies of the ring isomer have been characterized in order to aid future experimental attempts at isolation. The prospects of isolating the ring isomer, however, are slim at best. The low barrier to dissociation (4.4 kcal mol^{-1} with TZ2P CCSD) precludes attempts at isolation from the chain isomer as the energy required for ring closure would drive the molecule to dissociation. Extension to higher levels of theory and inclusion of ZPVE corrections questions the existence of any barrier whatsoever. While the barriers from the *trans*-chain isomer to the $N_2O + N_2$ and *trans*/*cis* transition states start out close to the barrier to ring dissociation at the DZP CISD level, neither the $N_2O + N_2$ nor the *trans*/*cis* transition states are as dramatically effected by improvements in basis set size and treatment of electron correlation. This may explain why the *trans*-chain isomer has been isolated and the ring has not. Although the ring isomer is the most stable N_4O isomer, and dissociation is accompanied by a release of 82.0 kcal mol^{-1} (TZ2P CCSD including ZPVE), even if isolation is successful, it may not be suitable as a high-energy-density material as the low barrier to dissociation is likely to prevent safe handling.

(60) This estimate does not take into account extending the basis set from TZ2P. Adding f-type functions, for example, could have a significant effect, as in going from DZP to TZ2P, or a small effect, as in adding diffuse functions to the DZP basis.

Acknowledgment. This research was supported by the U.S. Air Force Office of Scientific Research, Grant AFOSR-95-1-0057. J.M.G. would like to thank Professor R. D. Harcourt for preprints and personal correspondence, Professor Paul von Ragué Schleyer for helpful discussions, and Dr. Wesley Allen for both helping this research along (normal mode figures and helpful discussions) and holding it back (CHM895F and ski trips).

JA9534157